Morphological and magnetic characteristics of monodispersed Co-cluster assemblies

S. Yamamuro,[a] K. Sumiyama, T. Kamiyama, and K. Suzuki
Institute for Materials Research, Tohoku University, Sendai 980-8577, Japan

(Received 19 August 1998; accepted for publication 12 August 1999)

Co-cluster-assembled films have been prepared using a size-controllable cluster beam deposition system, by which monodispersed Co clusters with a mean diameter, $d=6-13$ nm are available. Their morphology and magnetic properties have been studied by scanning electron microscopy (SEM), small-angle x-ray scattering (SAXS) and magnetization measurements. The SEM images show that the film has a porous structure consisting of fine grains without a columnar texture and its density is about 25% of the bulk Co. The SAXS measurements indicate that monodispersivity of the incident clusters is maintained through their assembling process only for $d=13$ nm. All the specimens exhibit ferromagnetic behavior at room temperature and the magnetic coercive field H_c rapidly increases with decreasing temperature: $H_c=168$ kA/m (2.1 kOe) at 5 K. Such an enhancement in H_c is ascribed to the exchange anisotropy which arises from the antiferromagnetic Co–oxide layers covering the Co clusters, and to the assemblies of single-domain ferromagnetic clusters with the structure modification and magnetic interaction among them. The monotonic increase in H_c at 300 K with increasing d is simply understood in terms of the single-domain particle theory. © *1999 American Institute of Physics.* [S0021-8979(99)04722-2]

I. INTRODUCTION

Nanometer-scale geometrical and chemical controls are important to obtain novel magnetic materials such as soft-magnetic nanocrystalline materials with a high magnetic flux density,[1–3] spring-hard magnets with a large energy product,[3,4] magnetically perpendicular thin films, etc.[3,5–7] Their nanometer-scale chemical and structural heterogeneity is usually formed by precipitation from supersaturated solid solution initially produced by vapor-, liquid-, and solid-quenching methods. Apart from these metallurgical and conventional methods, by which the concentration and morphology cannot be independently controlled, laser or electron beam micro/nanolithography techniques permit the fabrication of submicrometer-scale magnetic dots, wires and arrays.[8,9] However, the lowest fabricated size obtained using lithography is about 20 nm. Submicrometer- to nanometer-sized fine particles have also been produced by inert gas condensation and colloidal methods,[10] and intensively studied for magnetic recording media and micromagnetic devices, although it is difficult to obtain monodispersed particles less than 10 nm by these methods.

The cluster-assembling method,[11] which directly deposits or arranges nanometer-sized clusters on a substrate, is a good alternative process to fabricate ideally nanostructure-controlled magnetic materials. Throughout the assembling process of the clusters, it is desirable to maintain the clusters initial size, structure and properties. In this context, we have constructed plasma–gas-condensation-type (PGC) cluster deposition equipment,[12–14] which is based upon plasma-glow-discharge vaporization (sputtering) and inert gas condensation.[15] This method can be used to produce refractive metal clusters because all metals can be sputtered. We have succeeded in producing monodispersed transition-metal clusters whose sizes are controlled between 6 and 13 nm in diameter and whose standard deviations are less than 10% of the mean sizes.[13,14] In our previous articles,[16–18] we presented the results of transmission electron microscopy (TEM) observations, *in situ* electrical resistivity and magnetization measurements in the early deposition stage of nanometer-sized Co clusters on substrates, and discussed the characteristic aspects of the assembling process in terms of two-dimensional percolation theory. It was found that a magnetic transition from superparamagnetic to ferromagnetic behavior starts prior to the geometrical and electrical percolation thresholds. This result strongly suggests the presence of a long range magnetic interaction between superparamagnetic Co clusters; magnetic dipole interactions are longer range than the interactions giving rise to the geometrical and electrical thresholds. Even far below the geometrical and/or electrical percolations, there are partial connections of clusters, which lead to the ferromagnetic behavior in these small Co-cluster assemblies.

When we produce a magnetic material whose size is smaller than about 50 nm, a multidomain structure changes to a single-domain structure. In such a small specimen, a magnetic domain wall is unstable because the interfacial energy loss exceeds the magnetostatic energy. If the magnetic anisotropy energy of a single-domain magnetic cluster is smaller than the thermal energy, the cluster becomes superparamagnetic at ambient temperature, obeying the statistical thermodynamics of classical spins. Looking at the rapid development of magnetic recording media, the memory unit size will be comparable to or smaller than 100 nm in the near

[a]Also with: Core Research for Evolutional Science and Technology (CREST) of Japan Science and Technology (JST) Corporation; electronic mail: yamamuro@imr.tohoku.ac.jp

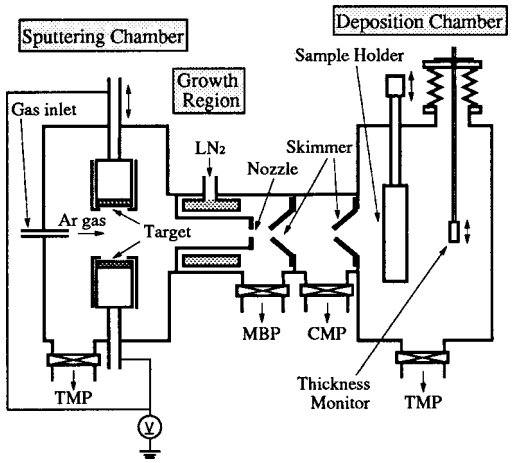

FIG. 1. Schematic diagram of the plasma-gas-condensation-type (PGC) cluster deposition system. TMP, MBP and CMP represent turbomolecular pump, mechanical booster pump, and compound molecular pump, respectively.

future. Superparamagnetism is a serious problem because the magnetization direction (the recorded information) is eliminated by thermal fluctuation. According to a simple theoretical calculation, the critical size of the transition from ferromagnetic to superparamagnetic states at room temperature is about 17 nm for an fcc Co particle, while it is about 10 nm for an hcp Co particle.[19] In our previous experiments concerning Co cluster deposition on substrates,[17] however, nearly isolated Co clusters with the mean diameter of 8.5 nm, mainly having an fcc structure, exhibit ferromagnetic behavior with a small hysteresis at 300 K. This is probably caused by the magnetic interaction between the clusters and/or the coexistence of a small amount of the hcp Co phase.

On the basis of these studies, we tried to produce rather thick films (three-dimensional cluster assemblies) from monodispersed Co clusters with the mean diameter of $d=6-13$ nm, and studied their morphological and magnetic features; the morphology by scanning electron microscopy (SEM), the medium range structure by small-angle x-ray scattering (SAXS) and the magnetic properties by a superconducting quantum interference device (SQUID) magnetometer.

II. EXPERIMENT

Figure 1 shows the PGC-type cluster deposition system, which mainly consists of a sputtering chamber, a growth region and a deposition chamber. A large amount of inert gas (pure Ar or Ar/He mixture) was steadily injected into the sputtering chamber from a gas inlet, and evacuated by a mechanical booster pump (MBP) through a small nozzle. In the sputtering chamber, two Co targets with 70 mm diameters were sputtered in a facing target mode at a high pressure of about 180 Pa. The input power for sputtering was 400 W. The growth region consists of a copper tube which was cooled by liquid nitrogen. This low temperature atmosphere causes the vaporized metal atoms to become supersaturated. The clusters formed in the growth region were ejected through the small nozzle and two skimmers by differential pumping, and then deposited onto a substrate fixed on a sample holder in the deposition chamber whose pressure was about 1×10^{-2} Pa. The substrate was maintained at room temperature during the deposition. The effective thickness of the deposited film, which corresponds to the average thickness of a dense film, was estimated at 100 nm using a crystal quartz thickness monitor. To check the accuracy of the thickness monitor for measuring the effective thickness of deposits, we examined the initial deposition stage of Co clusters on TEM microgrids by TEM and measured the cluster coverage by an image analysis of a TEM micrograph.[18] Assuming that spherical Co clusters with the diameter d are randomly placed on the substrate without any overlapping, we can calculate the effective thickness t from the cluster coverage p, using the relation of $t=(2d/3)p$. We found that the estimated effective thickness is about 40% smaller than the monitored thickness for all the specimens. Taking into account a lot of partial overlapping of the clusters in the real specimens, however, such a reduction of the estimated effective thickness will be attributable to the overlapping of the clusters because it makes an apparent cluster coverage, i.e., an apparent amount of the deposited clusters, small.

We controlled the cluster size by varying the Ar gas flow rate V_{Ar} and He gas flow rate V_{He}. With decreasing V_{Ar} from 8.3×10^{-6} (500 sccm) to $5.0\times10^{-6}\,\mathrm{m^3/s}$ (300 sccm), the mean cluster diameter decreases from 13 to 8.5 nm. However, the deposition rate rapidly decreases with decreasing V_{Ar}: smaller clusters cannot be massively produced in a pure Ar gas atmosphere. This is caused by a decrease in the cluster formation probability because the number of collisions among sputtered metal atoms decreases with increasing V_{Ar} (i.e., P_{Ar}). To overcome this problem, it is useful to mix He gas with Ar gas, leading to efficient cooling of the sputtered metal atoms due to the high thermal conductivity of the He gas. By mixing $V_{\mathrm{He}}=9.2\times10^{-6}\,\mathrm{m^3/s}$ (550 sccm) with $V_{\mathrm{Ar}}=4.2\times10^{-6}\,\mathrm{m^3/s}$ (250 sccm), for example, the mean cluster size could be decreased to 6 nm. To minimize the oxidation of the deposited films, we covered the specimens with carbon films of about 10 nm thickness.

We observed the morphology of the deposited films on silicon wafer substrates with a high-resolution scanning electron microscope (JEOL: JSM-6320F) operating at 3 kV. Prior to the deposition, the silicon wafers were cleaned by the RCA method[20] to eliminate contaminations and surface oxide layers using $NH_4OH/H_2O_2/H_2O$ and $HCl/H_2O_2/H_2O$ solutions. SAXS measurements were performed for the 200-nm-thick films deposited on mica substrates using a point focused Cu$K\alpha$ beam which was monochromatized by a small piece of pyrolytic graphite and then collimated by two apertures (0.5 mm×0.5 mm). Scattered x-ray intensity was detected by an imaging plate as two-dimensional data, which were then transferred into the one-dimensional data by circular averaging. We measured magnetization curves for the films deposited on polyimide film substrates using a SQUID magnetometer (Quantum Design Co.: MPMS-5).

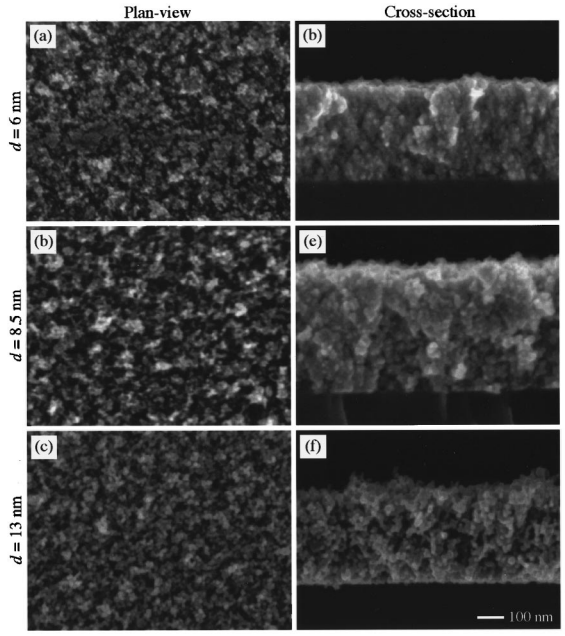

FIG. 2. Plan-view and cross-sectional scanning electron microscopy (SEM) images of the Co-cluster-assembled films with the mean cluster diameter, $d=6$, 8.5, and 13 nm. The effective thickness of the deposited film is 100 nm.

III. RESULTS

The external appearance of the Co-cluster assemblies is sooty, without any metallic luster. This is a typical characteristic of a thin film consisting of fine particles or clusters.[11] Electron diffraction measurements for Co clusters deposited on TEM microgrids indicate that the fcc phase is predominant for $d=6$ nm, while the fraction of the film that has an hcp phase gradually increases with increasing d.[21] This trend is qualitatively consistent with the result by Kitakami *et al.*[22] Figures 2(a)–2(f) show the plan-view and cross-sectional SEM images of the Co-cluster-assembled films with $d=6$, 8.5 and 13 nm, deposited on silicon wafer substrates. The plan-view images reveal very bumpy film surfaces containing inhomogeneous aggregations of Co clusters. In the cross-sectional images, we detect no distinct columnar structure (texture) as has been observed in thin films deposited by thermal evaporation or sputtering.[23] Instead, we observe a random stacking of Co clusters. Individual Co clusters are distinguishable for $d=13$ nm, while they are not so sharp for $d=6$ and 8.5 nm. This suggests that smaller clusters more easily coalesce to form larger particles because a cluster's melting point decreases with decreasing size.[24] Moreover, the film thickness estimated from the cross-sectional SEM image is 350–450 nm, although the planned thickness was 100 nm. This implies that the cluster-assembled films are very porous, being consistent with the results of the plan-view images.

Figure 3 shows the SAXS spectra of the Co-cluster assemblies with $d=6$, 8.5 and 13 nm deposited on mica substrates. The scattering intensity $I(h)$increases exponentially with decreasing scattering vector h below 1 nm^{-1}, indicating the presence of nanometer-scale electron-density fluctuation in these specimens. In particular, the SAXS spectrum for

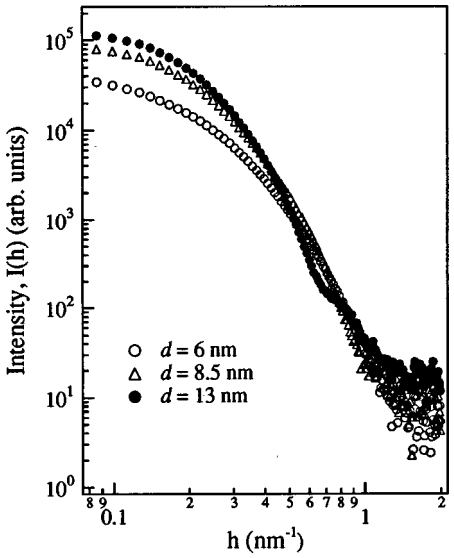

FIG. 3. Small-angle x-ray scattering (SAXS) intensity $I(h)$, vs the scattering wave vector h for the Co-cluster-assembled films with the mean cluster diameter, $d=6$, 8.5, and 13 nm.

$d=13$ nm reveals an oscillatory decay for $h=0.2$–1.0 nm^{-1}. This arises from the monodispersivity of the Co clusters.[25] However, the scattering intensities for $d=6$ and 8.5 nm reveal no oscillation, indicating that the deposited Co clusters do not maintain their initial monodispersivity after deposition.

Figure 4 shows a typical Guinier plot [$\log I(h)$ vs h^2] for the specimen with $d=6$ nm. The measured spectrum (the solid circles) exhibits a curved manner, indicating that the specimen consists of different size scatters. To estimate the gyration radius R_g of the scatters, the spectrum was analyzed by the Fankuchen method,[26] which assumes that $I(h)$ is comprised of the sum of multilines corresponding to different size scatters. The Guinier plot for $d=6$ nm provides two

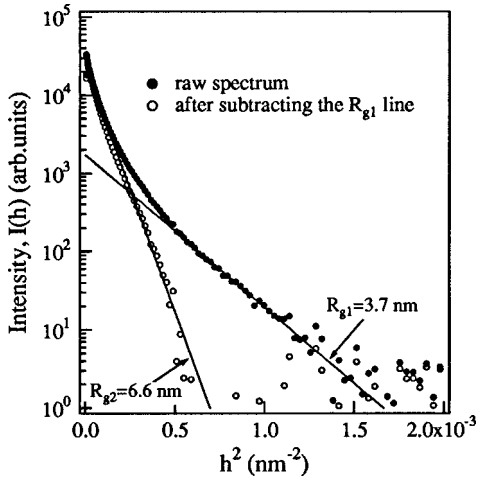

FIG. 4. Guinier plot [$\log I(h)$ vs h^2] of the SAXS spectrum for the Co-cluster-assembled film with the mean cluster diameter, $d=6$ nm. The solid circle is a raw spectrum and the open circle is a retained spectrum after subtracting the straight line corresponding to R_{g1} from the raw spectrum. The straight lines fitted to each spectra correspond the gyration radii R_{g1} and R_{g2}.

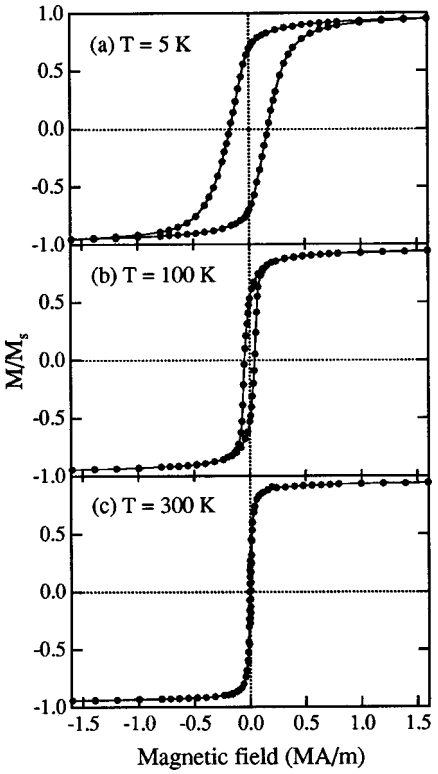

FIG. 5. Magnetization curves (relative magnetization M/M_s vs applied field H, along the in-plane direction) measured at 5, 100 and 300 K for the Co-cluster-assembled films with the mean cluster diameter $d=6$ nm.

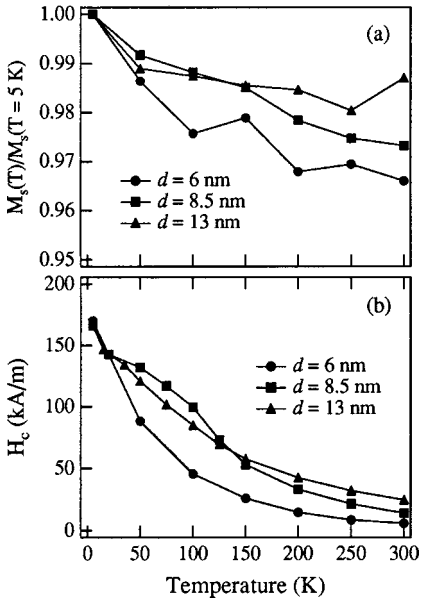

FIG. 6. Temperature dependence of: (a) relative magnetization M/M_s and (b) magnetic coercive field H_c along the in-plane direction for the Co-cluster-assembled films with the mean cluster diameter, $d=6$, 8.5 and 13 nm.

gyration radii: $R_{g1}=3.7$ nm and $R_{g2}=6.6$nm; R_{g1} and R_{g2} probably correspond to the incident clusters and aggregations of clusters, respectively.

Figure 5 shows typical magnetization curves (the relative magnetization M/M_s versus magnetic field H) along the in-plane direction of the Co-cluster-assembled film with $d=6$ nm at different temperatures: $T=5$, 100 and 300 K. The M_s value is defined as a magnetization value measured at $T=5$ K and $H=4$MA/m (50 kOe). The film exhibits ferromagnetic characteristics at $T\leqslant 300$: a magnetic saturation and hysteresis. The magnetization curve becomes magnetically soft with increasing T.

Figure 6(a) shows the T dependence of $M_s(T)/M_s(T=5$ K) for $d=6$, 8.5 and 13 nm. The $M_s(T)/M_s(T=5$ K) values for all the specimens gradually decrease with increasing T, however, its decreasing ratio from $T=5$ to 300 K is only 2%–3% irrespective of d, indicating that M_s is insensitive to T and d in these ranges. In the present experiments, it is difficult to determine the saturation magnetization per Co mass directly from the magnetization curves at high magnetic field, because we were unable to measure the weight of the deposited Co clusters due to their very small amount. However, it was confirmed that the magnetic moment per Co atom in the clusters is in good agreement with that in the bulk Co by a Langevin fitting to the magnetization curves for isolated Co clusters with $d=6$ nm, which were deposited on a substrate with the average thickness of 1 nm.[17]

As shown in Fig. 6(b), the coercive field H_c rapidly increases with decreasing T; for $d=6$ nm, for instance, H_c increases from 6 kA/m (75 Oe) to 168 kA/m (2.1 kOe) when T is decreased from 300 to 5 K. Although H_c is almost independent of d at $T<20$ K, it becomes larger for larger sized clusters at $T=300$ K; the H_c values at $T=300$ K are 6 kA/m (75 Oe), 14 kA/m (180 Oe) and 25 kA/m (315 Oe) for the respective d values of 6, 8.5 and 13 nm. The large H_c value at low temperature is ascribed to both an intrinsic property of ferromagnetic single-domain particles and an extrinsic property of the exchange anisotropy.[27] The latter originates from the presence of an antiferromagnetic oxide layer covering the ferromagnetic cluster.[27,28]

To confirm the presence of the exchange anisotropy, we measured the magnetization curves under zero-field-cooled (ZFC) and field-cooled (FC) conditions. In the latter case, we cooled the specimens from $T=300$ to 5 K with $H=800$kA/m (10 kOe). Figure 7 shows typical ZFC and FC magnetization curves for $d=6$ nm at $T=5$ K. A negative shift in the hys-

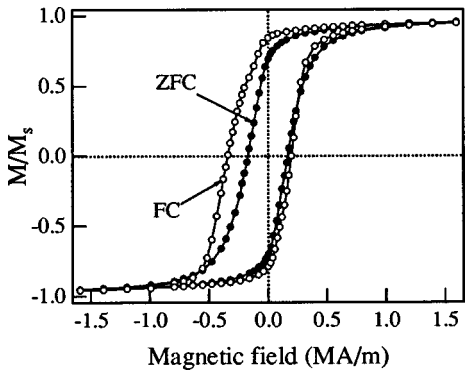

FIG. 7. Zero-field-cooled (ZFC) and field-cooled (FC) magnetization curves (relative magnetization M/M_s vs applied field H along the in-plane direction) at 5 K for the Co-cluster-assembled films with the mean cluster diameter $d=6$ nm. The specimens were cooled from 300 to 5 K with/without $H=800$kA/m (10 kOe).

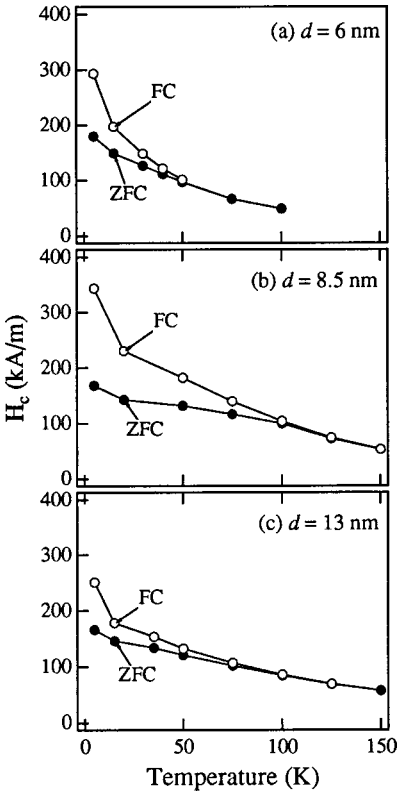

FIG. 8. Magnetic coercive field H_c of the zero-field-cooled (ZFC) and field-cooled (FC) magnetization curves of the Co-cluster-assembled films as a function of temperature: (a) the mean cluster diameter $d=6$ nm, (b) $d=8.5$ nm, and (c) $d=13$nm. The H_c value of the FC specimen is defined as the average of the positive and negative field values.

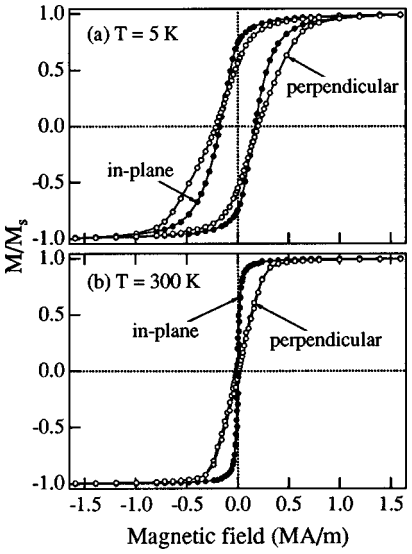

FIG. 9. Magnetization curves (relative magnetization M/M_s vs applied field H) along the in-plane and perpendicular directions of the Co-cluster-assembled films with the mean cluster diameter $d=6$ nm at (a) 5 K and (b) 300 K.

teresis loop along the field axis is detected in the FC specimen in comparison with the symmetric feature in the ZFC one; the exchange bias field for the FC specimen is 72 kA/m (0.9 kOe). This suggests the presence of a surface layer of CoO on the clusters. We also measured the magnetization curves of both ZFC and FC specimens at several temperatures after measuring at $T=5$K. Figures 8(a)–8(c) show the H_c values for the Co-cluster assemblies with $d=6$, 8.5 and 13 nm as a function of T. For the FC specimens, H_c is defined as the average of the positive and negative field values. The difference in H_c between the ZFC and FC specimens becomes more significant with decreasing T. Such a bifurcation effect starts at $T=50$ K for $d=6$ nm and at $T=100$ K for $d=8.5$ and 13 nm. This feature indicates that the exchange anisotropy appears/disappears at these temperatures. We obtained the highest H_c value of 344 kA/m (4.3 kOe) at $T=5$ K for the FC specimen with $d=8.5$ nm. In addition, the exchange bias field was large for $d=8.5$ nm; it achieved 200 kA/m (2.5 kOe) at $T=5$K.

Figures 9(a) and 9(b) show the magnetization curves measured at $T=5$ and 300 K along the in-plane and perpendicular directions of the Co-cluster-assembled film with $d=6$ nm. The magnetization along the in-plane direction is more easily saturated than that along the perpendicular direction due to the shape anisotropy of the film as a macroscopic platelet. However, the difference between the in-plane and perpendicular directions is not as significant as those in the Co thin films produced by sputtering or thermal evaporation. This indicates that the Co-cluster-assembled films are magnetically rather isotropic in comparison with the conventionally vapor-deposited films due to the random stacking of small clusters without preferential orientation.

IV. DISCUSSION

As described in Sec. III, the coercive field H_c is strongly influenced by the cluster size, temperature, and surface oxidization of the clusters. These results indicate that H_c sensitively reflects the nanostructural characteristics. Thus, we focused on the H_c behavior to characterize the specific features of the present Co-cluster-assembled films. In general, the d dependence of H_c in nanocrystalline magnetic materials is explained in terms of the competition between the ferromagnetic exchange and anisotropy fields. In bulk ferromagnetic materials consisting of large grains, the magnetization process is dominated by the domain wall movement, and H_c is roughly proportional to d^{-1}.[29] On the contrary, small H_c values have been observed in nanocrystalline ferromagnetic materials produced via annealing of amorphous alloys.[30] Since this superior soft-magnetic property is very useful as mentioned in Sec. I, there have been many experimental and theoretical studies of these materials.[1–3,31] It has been proposed[29] that the local magnetocrystalline anisotropy is averaged out by the exchange interaction between the nanometer-sized magnetic grains, leading to a small net anisotropy. In a small d range, H_c increases in proportion to d^6 as follows:[31]

$$H_c = p_c \frac{K_1^4 d^6}{M_s A^3}, \tag{1}$$

where K_1 is the magnetic anisotropy constant, and A is the exchange stiffness constant. The p_c value is a constant defined by the crystalline symmetry, orientation, and shape of the grains: for example, p_c is 0.64 and 0.96 for ensembles of

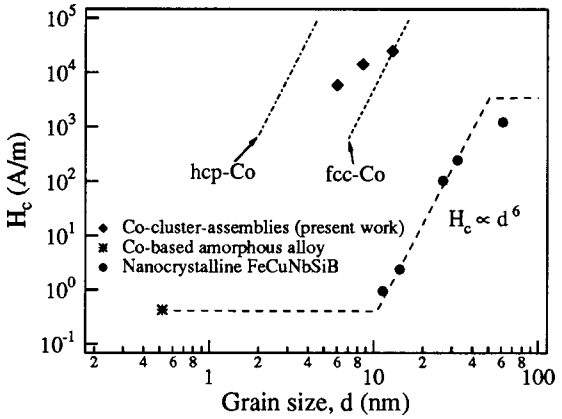

FIG. 10. Magnetic coercive field H_c as a function of the grain diameter d for the Co-cluster-assembled films and nanocrystalline materials. The dotted and dash-dotted lines indicate the results for fcc and hcp Co nanocrystalline materials estimated from Eq. (1), respectively.

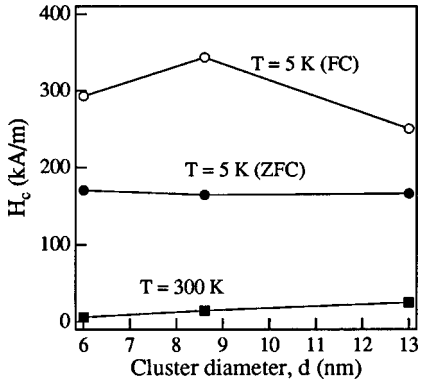

FIG. 11. Magnetic coercive field H_c of the zero-field-cooled (ZFC) and field-cooled (FC) magnetization curves for the Co-cluster-assembled films as a function of the mean cluster diameter d.

randomly oriented cubic-crystal particles (fcc Co) and uniaxial particles (hcp Co), respectively.[32] Using these ideas, we tried to clarify the characteristic features of the cluster-assembled films.

Figure 10 shows the d dependence of H_c at $T=300$ K for the present Co-cluster-assembled films, together with those for other nanocrystalline materials.[31] The H_c values of the Co-cluster-assembled films increase from 6 kA/m (75 Oe) to 25 kA/m (315 Oe) with increasing d from 6 to 13 nm, indicating that the thermal fluctuation is more marked for the smaller cluster assembly. This is mainly due to the single domain particle regime and partially due to the increase in the ratio of hcp to fcc Co with increasing d. It is also noted that the H_c values for the present Co-cluster-assembled films are much higher than those for the usual nanocrystalline materials. We also drew the lines for the fcc (dotted line) and hcp Co nanocrystals (dash-dotted line) estimated from Eq. (1) using the reported values of $A=1.3\times10^{-11}$ J/m, $K_1=-7.5\times10^4$ J/m^3 and $M_s=1.8$ Wb/m^2 (1420 G) for the bulk fcc Co and $A=1.3\times10^{-11}$ J/m, $K_1=4.6\times10^5$ J/m^3 and $M_s=1.8$ Wb/m^2 (1420 G) for the bulk hcp Co.[33] The data are located between the two lines estimated for the fcc and hcp Co nanocrystalline films. However, the slope of the data is estimated to be 1.8, which is much smaller than the expected value of 6. This implies that the magnetically coupled region is three dimensionally nonuniform due to the contribution of the magnetic dipole interaction among the clusters.[34,35]

According to the simple theory on a random assembly of single-domain particles, the magnetic coercive field is expressed as $H_c^{\mathrm{I}}=p_c K_1/M_s$.[29,36] Thus, H_c^{I} is independent of d in this relation; H_c is about 27 kA/m (0.34 kOe) for the fcc Co clusters and 248 kA/m (3.1 kOe) for the hcp Co clusters using the above-mentioned values of p_c, K_1 and M_s. Moreover, since H_c depends on a packing density of magnetic particles, the observed H_c is empirically related to the ideal H_c^{I} as follows: $H_c=(1-P)\cdot H_c^{\mathrm{I}}$, where P is the packing fraction of the clusters.[32] The P value estimated from Fig. 2 is about 0.25 (=100 nm/400 nm), resulting in $H_c=21$ kA/m (0.26 kOe) for the fcc Co-cluster assemblies and 184 kA/m (2.3 kOe) for the hcp ones. At $T=300$ K, the H_c values observed for the present Co-cluster assemblies are comparable to the theoretically estimated ones for a porous assembly of single-domain fcc Co clusters.

Figure 11 shows the H_c values for FC ($H=800$ kA/m) and ZFC specimens measured at $T=5$ and 300 K as a function of d. For the ZFC specimen, the H_c values at $T=5$ K are much larger than those at $T=300$ K. As described in Sec. III, such a large enhancement in H_c is ascribed to the exchange anisotropy effect; the antiferromagnetic coupling in the interface between the ferromagnetic core and the antiferromagnetic shell (surface layer) gives rise to an extrinsic unidirectional anisotropy because the antiferromagnetic phase does not easily align along an applied field direction. According to our TEM experiments, the thickness of the oxide surface layer is less than 1–2 nm and diffuse diffraction rings indexed to the reflections of CoO are detected in electron diffraction patterns.[21] As shown in Figs. 8(a)–8(c), however, the exchange anisotropy effect disappears at $T=50$ K for $d=6$ nm and $T=100$ K for $d=8.5$ and 13 nm, although it has been reported that the Néel temperature T_N for CoO is 290 K.[27] Since T_N for Co_3O_4 (=40 K) is much lower than that for CoO, one possible reason for the depression of the exchange anisotropy effect is the coexistence of CoO and Co_3O_4 surface layers in the present Co-cluster-assembled films, as has been reported by Gangopadhyay *et al.*[27] Moreover, recent extensive studies on an exchange coupling between ferromagnetic and antiferromagnetic layers also revealed that the exchange anisotropy effect is considerably weakened with decreasing antiferromagnetic layer thickness, particularly below a few nm.[37–39] Since the thin oxide layer leads to a thermal fluctuation in its antiferromagnetism, it is highly plausible that the oxide surface layers become superparamagnetic even below 290 K and the exchange anisotropy is weakened even at low temperatures.[40]

At $T=5$ K, the H_c values for the FC specimens are much larger than that for the ZFC ones. In particular, H_c provides a peak value of about 344 kA/m (4.3 kOe) for $d=8.5$ nm, although the H_c values for the ZFC specimens are independent of d. This result is reproducible for the other specimens with a similar cluster size. Thus, it can be said that the exchange anisotropy is enhanced at around $d=8.5$

nm, suggesting that the exchange anisotropy is maximized at a certain ratio of the interfacial area of the ferromagnetic/antiferromagnetic phases to the ferromagnetic core volume.

The H_c values at $T=5$K are still about 168 kA/m (2.1 kOe) for the ZFC specimens in which the exchange anisotropy effect is randomized. This value is comparable to that theoretically estimated for the single-domain hcp Co-particle assembly. The structure modification, such as coexistence of the hcp Co phase with the fcc one and/or accumulation of hcp/fcc stacking faults, also induces a magnetic anisotropy. In ferromagnetic cluster assemblies, H_c is also enhanced by a magnetic interaction among these clusters. When particles are connected to form a chain and the magnetic moments between the adjacent particles are noncollinear, the magnetization process is described by a fanning mode.[41] This mechanism leads to a large H_c value of about 216 kA/m (2.7 kOe) as observed in the present Co-cluster assemblies. Moreover, it has been proposed that such an enhancement in the magnetic anisotropy is associated with the marked influence of the low symmetric surface atoms, lattice defects in these small clusters.[42] To understand the origin of the large H_c value in the present nanometer-sized Co-cluster-assembled films, we plan to study the more precise structure and magnetic properties of Co clusters through high-resolution TEM observations and the magnetic measurements of forcedly oxidized Co clusters.

V. CONCLUSION

Using the PGC-type cluster deposition system, we have produced Co-cluster-assembled films consisting of monodispersed Co clusters with a mean diameter of $d=6-13$ nm. SEM, SAXS, and magnetization measurements were performed to study their nanometer-scale morphology and magnetic properties. Random stacking of Co clusters leads to a very porous film structure whose density is about 25% of the bulk Co. These films are comprised of inhomogeneously aggregated clusters without a columnar texture. Only the larger Co-clusters ($d=13$ nm) of our specimens maintain their initial monodispersivity throughout their assembly process. The coercive field H_c at 300 K monotonically increases from 6 kA/m (75 Oe) to 25 kA/m (315 Oe) with increasing d from 6 to 13 nm, being comparable to the values theoretically estimated for a porous assembly of single-domain fcc Co clusters. On the other hand, the H_c value rapidly increases with decreasing temperature: $H_c=168$ kA/m (2.1 kOe) at 5 K. Such a large H_c value is ascribed to the exchange anisotropy arising from the antiferromagnetic Co–oxide surface layer, and also to the assemblies of single-domain Co clusters with the structure modification and magnetic interaction among them.

ACKNOWLEDGMENTS

The authors thank Dr. M. Sakurai for useful discussion, and E. Aoyagi and Y. Hayakawa for their helps in the SEM observations. This work was supported by Core Research for Evolutional Science and Technology (CREST) of Japan Science and Technology (JST) Corporation, and partly by a Grant-in-Aid for Scientific Research A1 (Grant No. 08505004). They were also indebted to the support from the Laboratory for Developmental Research of Advanced Materials in their Institute.

[1] *Nanomagnetism*, edited by A. Hernando, NATO ASI Series E: Applied Science, Vol. 247 (Kluwer Academic, Dordrecht, 1993).
[2] D. L. Leslie-Pelecky and R. D. Rieke, Chem. Mater. **8**, 1770 (1996).
[3] *Magnetic Hysteresis in Novel Magnetic Materials*, edited by G. C. Hadjipanayis, NATO ASI Series E: Applied Science, Vol. 338 (Kluwer Academic, Dordrecht, 1997).
[4] E. F. Kneller, IEEE Trans. Magn. **27**, 3588 (1991).
[5] K. Ouchi, Trans. Mater. Res. Soc. Jpn. **15B**, 709 (1994).
[6] J. C. Lodder, J. Magn. Magn. Mater. **159**, 238 (1996).
[7] M. T. Johnson, P. J. H. Bloemen, F. J. A. den Broeder, and J. J. de Vries, Rep. Prog. Phys. **59**, 1409 (1996).
[8] S. Y. Chou, P. R. Krauss, and L. Kong, J. Appl. Phys. **79**, 6101 (1996).
[9] P. D. Ye, D. Weiss, R. R. Gerhardts, and H. Nickel, J. Appl. Phys. **81**, 5444 (1997).
[10] *Nanomaterials: Synthesis, Properties and Applications*, edited by A. S. Edelstein and R. C. Cammarata (Institute of Physics, Bristol, 1996).
[11] P. Melinon *et al.*, Int. J. Mod. Phys. B **9**, 339 (1995).
[12] S. Yamamuro, M. Sakurai, T. J. Konno, K. Sumiyama, and K. Suzuki, AIP Conf. Proc. **416**, 491 (1998).
[13] S. Yamamuro, M. Sakurai, K. Sumiyama, and K. Suzuki, Supramol. Sci. **5**, 239 (1998).
[14] S. Yamamuro, K. Sumiyama, and K. Suzuki, J. Appl. Phys. **85**, 483 (1999).
[15] H. Haberland, M. Karrais, M. Mall, and Y. Thurner, J. Vac. Sci. Technol. A **10**, 3266 (1992).
[16] S. Yamamuro, K. Sumiyama, T. Hihara, and K. Suzuki, J. Phys. Soc. Jpn. **68**, 28 (1999).
[17] S. Yamamuro, K. Sumiyama, and K. Suzuki, Mater. Trans., JIM (submitted).
[18] S. Yamamuro, T. Hihara, K. Sumiyama, and K. Suzuki, J. Phys.: Condens. Matter **11**, 3247 (1999).
[19] O. Kitakami, T. Sakurai, Y. Miyashita, Y. Takeno, Y. Shimada, H. Takano, H. Awano, K. Ando, and Y. Sugita, Jpn. J. Appl. Phys., Part 1 **35**, 1724 (1996).
[20] W. Kern and D. A. Puotineu, RCA Rev. **1970**, 187.
[21] S. Yamamuro, K. Sumiyama, and K. Suzuki, (unpublished).
[22] O. Kitakami, H. Sato, Y. Shimada, F. Sato, and M. Tanaka, Phys. Rev. B **56**, 13849 (1997).
[23] J. A. Thornton, Annu. Rev. Mater. Sci. **7**, 239 (1977).
[24] Ph. Buffat and J.-P. Borel, Phys. Rev. A **13**, 2287 (1976).
[25] A. Guinier and G. Fournet, *Small-Angle Scattering of X-Rays* (Wiley, New York, 1955), p. 20.
[26] T. Kamiyama, N. Yoshida, and K. Suzuki, Bull. Inst. Chem. Res., Kyoto Univ. **72**, 225 (1992).
[27] S. Gangopadhyay, G. C. Hadjipanayis, C. M. Sorensen, and K. J. Klabunde, IEEE Trans. Magn. **28**, 3174 (1992).
[28] W. H. Meiklejohn and C. P. Bean, Phys. Rev. **105**, 904 (1957).
[29] A. H. Morrish, *The Physical Principles of Magnetism* (Wiley, New York, 1965), p. 354.
[30] Y. Yoshizawa, S. Oguma, and K. Yamauchi, J. Appl. Phys. **64**, 6044 (1988).
[31] G. Herzer, IEEE Trans. Magn. **26**, 1397 (1990).
[32] R. M. Bozorth, *Ferromagnetism* (IEEE, New York, 1978), p. 831.
[33] F. Sato, N. Tezuka, T. Sakurai, and T. Miyazaki, J. Magn. Soc. Jpn. **17**, 886 (1993).
[34] H. Hoffmann, IEEE Trans. Magn. **MAG–9**, 17 (1973).
[35] K. Suzuki, J. M. Cadogan, V. Sahajwalla, A. Inoue, and T. Masumoto, J. Appl. Phys. **79**, 5149 (1996).
[36] E. C. Stoner and E. P. Wohlfarth, Philos. Trans. R. Soc. London **240**, 599 (1948).
[37] N. C. Koon, Phys. Rev. Lett. **78**, 4865 (1997).
[38] M. J. Carey, A. E. Berkowitz, J. A. Borchers, and R. E. Erwin, Phys. Rev. B **47**, 9952 (1993).
[39] D. V. Dimitrov, S. Zhang, J. Q. Xiao, G. C. Hadjipanayis, and C. Prados, Phys. Rev. B **58**, 12090 (1998).
[40] S. Gangopadhyay, G. C. Hadjipanayis, C. M. Sorensen, and K. J. Klabunde, J. Appl. Phys. **73**, 6964 (1993).
[41] I. S. Jacobs and C. P. Bean, Phys. Rev. **100**, 1060 (1955).
[42] M. Respaud *et al.*, Phys. Rev. B **57**, 2925 (1998).